Final Report

Grant No. DE-FG02-01ER45907

1 Atomic layer-by-layer growth by laser MBE from separate targets

Two most effective film deposition techniques for oxides are reactive MBE [1] and laser MBE [2, 3]. Using reactive MBE, Prof. Darrell Schlom (formerly at Penn State and currently at Cornell) has shown stoichiometry control and crystalline perfection in $SrTiO_3$ films on $SrTiO_3$ by alternately growing each atomic layer [4]. Exceptionally high quality $BaTiO_3/SrTiO_3$ superlattices with nanoscale dimensions have been grown by reactive MBE [5], which allowed us to study nanoscale ferroelectricity using UV Raman spectroscopy [6]. Laser MBE carries out pulsed laser deposition (PLD) under high vacuum conditions similar to that in reactive MBE, aided with a differentially pumped RHEED system [3]. Most reports on the 2D electron gas at the $LaAlO_3/SrTiO_3$ interface, one of the most active areas in contemporary condensed matter physics, employs laser MBE for the film growth [7].

Most works of laser MBE use compound targets (see Fig. 1), for example, using a $SrTiO_3$ target to grow $SrTiO_3$ films. All elements in the oxide compound are ablated at once and the film grows in a unit-cell-by-unit-cell manner. The oscillation of the RHEED intensity corresponds to different stages of coverage of the one unit cell thick layer. The approach is similar to the codeposition mode of reactive MBE, and lacks the stoichiometry control capability of reactive MBE with alternate monolayer growth. Homoepitaxial growth of $SrTiO_3$ on $SrTiO_3$ by laser MBE from $SrTiO_3$ targets frequently shows non-stoichiometry and lattice defects evidenced by a lattice expansion [8].

In order to achieve atomic layer-by-layer growth, it is necessary to carry out laser MBE from separate oxide targets, for example growing $SrTiO_3$ from SrO and TiO_2 targets (see Fig. 2). The process mimics the alternate monolayer growth in reactive MBE. The targets are switched back and forth to be ablated by

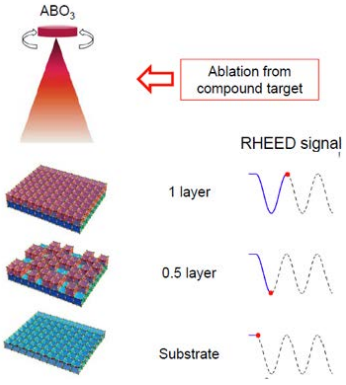

Figure 1: Laser MBE from one compound target. All elements in the ABO_3 are ablated at once, and the film grows in a unit-cell-by-unit-cell manner.

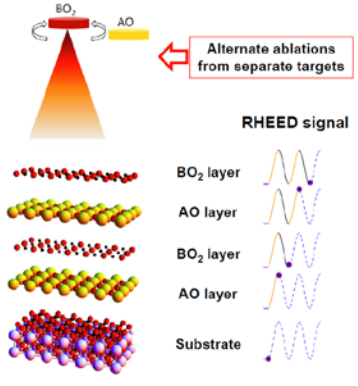

Figure 2: Laser MBE from separate oxide targets AO and BO_2. The targets are ablated alternately, and the film grows in an atomic layer-by-layer manner.

the pulsed laser beam alternately, thus depositing one atomic layer at a time. The RHEED intensity recovers its original value when a complete SrTiO3 layer is grown after the depositions of one SrO layer and one TiO_2 layer. Similar approach has been demonstrated by Kanai et al. in the early 1990s [9], but it is not commonly practiced today. However, it is only possible for laser MBE to match the extraordinary stoichiometry control and crystalline perfection demonstrated by the reactive MBE by ablating from separate oxide targets.

In this project period, the PI has relocated from Penn State University to Temple University, and in the process acquired a state-of-the-art laser MBE system. Using this equipment, we have investigated the homoepitaxial deposition of $SrTiO_3$ on $SrTiO_3$ substrate from SrO and TiO_2 targets and showed that by using separate oxide targets, laser MBE can achieve the same level of stoichiometry control as the reactive MBE.

The first critical step for atomic layer-by-layer growth of oxide films is the preparation of atomically smooth single crystal substrates with specific surface termination. Based on a process first developed by Kawasaki et al. [10] and later optimized by Koster et al. [11], we have prepared TiO_2-terminated $SrTiO_3$ substrates for the homoepitaxial growth of $SrTiO_3$. An AFM image of a treated $SrTiO_3$ substrate is shown in Fig. 3. The treatment involves soaking the substrate in deionized water so that the SrO-terminated domains form a Sr-hydroxide complex while the TiO_2-terminated layers remain chemically stable, subsequently dipping the substrate in a buffered hydrofluoric (BHF) solution so that the Sr-hydroxide complex is dissolved, and finally annealing the substrate in flowing oxygen to remove the remnants of the previous treatments and facilitate recrystallization. The stripes of different colors in the image are steps with atomically smooth top surface. As seen from a surface scan shown as the inset, the height of the steps is about 0.4 nm, or one unit cell.

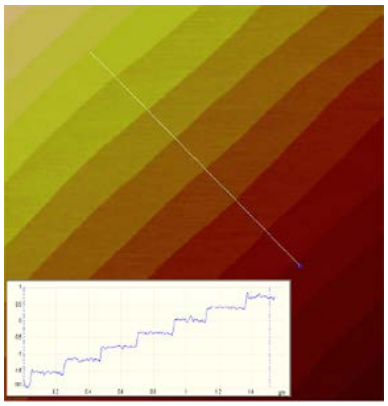

Figure 3: AFM image of a treated $SrTiO_3$ substrate. Inset: A surface scan along the white line.

The film growth conditions are the following: oxygen pressure during growth – $4x10^{-4}$ Pa; laser energy density – 2 J/cm2; repetition rate – 3 Hz; and substrate temperature – 720◦C. For each SrO layer, 90 laser pulses were fired on the SrO target. For each TiO_2 layer, 126 laser pulses were fired on the TiO_2 target. The two targets were moved to the front of the laser beams alternately such that the SrO and TiO_2 layers were deposited alternatively one atomic layer at a time. To change stoichiometry, the numbers of pulses on each target were adjusted. The switch of the targets took 6 seconds.

Figure 4 shows the RHEED intensity as a function of time for the (01) streaks along the [110] azimuth during the growth of three $SrTiO_3$ films of different stoichiometry: (a) 5% Sr rich, (b) stoichiometric, and (c) 5% Sr poor. The oscillation pattern in Fig. 4(b) with a stable RHEED intensity is characteristic of the Sr:Ti stoichiometry and full monolayer dosage for each layer [4]. For the case of excess strontium [Fig. 4(a)], the RHEED intensity passes a peak before switching to the TiO_2 target. For the case of strontium

deficiency [Fig. 4(c)], the ablation of the TiO_2 target starts before the RHEED intensity reaches a maximum, therefore the peak maxima decrease in intensity over time. These characteristics were used to monitor and control the growth of the film in order to achieve desired stoichiometry and crystallinity. To obtain full monolayer dosage in each layer and 1:1 stoichiometry, the RHEED intensity must be diligently observed and the number of pulses for each layer carefully adjusted.

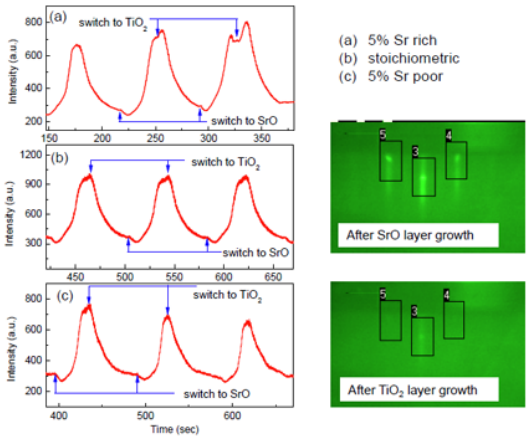

Figure 4: RHEED intensity during growth of $SrTiO_3$ films from separate SrO and TiO_2 targets. (a) Sr rich, (b) stoichiometric, and (c) Sr poor.

The $SrTiO_3$ films of different stoichiometry were characterized by x-ray diffraction measurement. Figure 5 shows θ-2θ scans around the (200) peak of 5 Sr1+xTiO3 films of 70 nm in thickness with (from top to bottom) x = 0.2, 0.1, 0 -0.1, and - 0.2, respectively. The strong peak from the $SrTiO_3$ substrate is marked by a vertical dashed line. The peaks from the films are broader and weaker than that of the substrate and marked by arrows. The figure clearly shows that when the film is off stoichiometry, either Sr rich or Sr poor, the lattice expands, leading to smaller θ angles for the diffraction peaks [8]. The further off stoichiometry is the film composition, the more the lattice expands, thus the larger the deviation between the film peak and the substrate peak. When the film has an exact 1:1 stoichiometry between Sr and Ti, however, the film peak overlaps with and is indistinguishable from that of the substrate. Around the film peaks intensity oscillations are seen, which correspond to the 70 nm film thickness and indicate smooth interfaces between the films and substrate. Again, when the film is stoichiometric, the oscillation is not visible because the deposited film and the substrate are indistinguishable from each other.

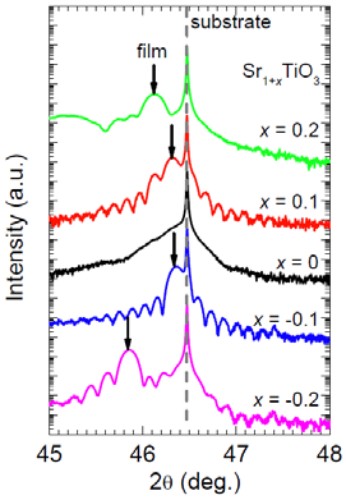

Figure 5: XRD θ-2θ scans around the (200) peak of 5 $Sr1+xTiO_3$ films. From top to bottom: x = 0.2, 0.1, 0 -0.1, and - 0.2.

The result in Fig. 5 is identical to that of atomic layer-by-layer growth of $SrTiO_3$ by Brooks et al. using reactive MBE (see Fig. 2 in Ref. [4]). In the case of reactive MBE, the stoichiometry is controlled by adjusting the shutter open times for the Sr and Ti sources, aided by the RHEED intensity oscillation. For laser MBE, we control the stoichiometry by adjusting the numbers of laser pulses fired on the SrO and TiO_2 targets with the help of RHEED intensity oscillation. Both techniques have achieved equally excellent stoichiometry control.

A question asked frequently by researchers is: Reactive MBE or Laser MBE? Our result indicates that in terms of precise control of growth at atomic layer level, the two techniques are identical if laser MBE is performed using separate oxide targets. There are differences between the two techniques: the energy of the flux is lower in reactive MBE than in laser MBE, and the oxygen

pressure range during growth/cooling is broader in laser MBE than in reactive MBE. While the effects of these differences need to be studied for specific materials, we are confident that laser MBE from separate oxide targets can produce the same extraordinarily high quality oxide thin films and heterostructures as reactive MBE has demonstrated.

2 Strain relaxation in $LaAlO_3$ films and its effect on the 2D electron gas at $LaAlO_3/SrTiO_3$ interface

The remarkable existence of a high-mobility 2D electron gas (2DEG) at the interface between $LaAlO_3$ film and TiO_2-terminated $SrTiO_3$ substrate [7, 12] as well as its remarkable properties such as superconductivity [13] and magnetism [14] have generated significant interest. The origin of the conducting interface layer has been heatedly debated [15, 16]. The most dominant explanation attributes it to polar catastrophe due to the polar discontinuity at the $LaAlO_3/SrTiO_3$ interface: the LaO+ and AlO_2 planes of $LaAlO_3$ are charged but the SrO and TiO_2 planes of SrTiO3 are neutral [17, 18]. In this picture, a divergence of the electric potential as the $LaAlO_3$ film grows is avoided when a charge of e/2 is transferred from the LaO+ plane to the TiO2 plane, giving rise to the 2DEG. A critical thickness of the $LaAlO_3$ film is needed so that the potential exceeds the bandgap of $SrTiO_3$, which has been observed [19]. Many other explanations of the conducting interface between LaAlO3 and $SrTiO_3$ have been proposed [15], including oxygen vacancies in $SrTiO_3$ [20], laser bombardment of $SrTiO_3$ surface [21], and interfacial mixing [22].

Since the 2DEG resides at the $SrTiO_3$ side of the interface, all explanations concern $SrTiO_3$. What effect can the $LaAlO_3$ layer have beyond that it needs to exceed the critical thickness to build up sufficient electric potential for the charge transfer to take place? Bell et al. have found that the mobility of the 2DEG decreases by nearly two orders of magnitude when the $LaAlO_3$ thickness increases from 5 to 25 unit cells [23]. By tunneling into the 2DEG through $LaAlO_3$, Singh-Bhalla et al. found that a potential did build up with $LaAlO_3$ thickness, possibly due to incomplete screening, before a Zener breakdown at about 20 unit cells [24].

In our work, the focus is on the strain and strain relaxation in the LaAlO3 film. It is difficult to measure strain in ultrathin films with thicknesses of only a few unit cells, and the state of strain near the $LaAlO_3/SrTiO_3$ interface is unknown. In the process to relocate from Penn State to Temple, the PI purchased a Bruker D8 DISCOVER system which has the capability of in-plane grazing incidence diffraction measurement. With this technique, the x-ray is scattered on lattice planes perpendicular to the sample surface, allowing direct determination of the in-plane lattice constant and lattice mismatch in very thin epitaxial layers. For thicker $LaAlO_3$ films, the reciprocal space mapping (RSM) technique was used.

$LaAlO_3$ film of different thicknesses were grown on TiO_2-terminated $SrTiO_3$ substrate by laser MBE from a $LaAlO_3$ single crystal target under the following conditions: oxygen pressure during growth – 4×10^{-4} Pa; laser energy density – 2 J/cm2; repetition rate – 1 Hz; and substrate temperature – 720◦C. The films grow epitaxially with c-axis normal to the substrate surface.

Figure 6 shows 2 GIXRD scans around the (200) plane diffraction for $LaAlO_3$ films of (a) 14, and (b) 35 unit cells in thickness and 2 reciprocal space maps around the $SrTiO_3$ (103) reflection for $LaAlO_3$ films of (c) 125, and (d) 250 unit cells in thickness. For the GIXRD data, no satisfactory fitting can be obtained if only one peak is assumed from the $LaAlO_3$ film, and two film peaks leads to good fit. For the thicker LaAlO3 films, a broad double spot is found for the $LaAlO_3$ film (around L = 3.12). Both the two-peak fitting in GIXRD for thinner films and the double spot in RSM for thicker films suggest that there are two layers of different in-plane lattice constants in the $LaAlO_3$ films. The in-plane lattice constants of $LaAlO_3$ films as a function of film thickness obtained from both measurements are shown in Fig. 7. Two in-plane lattice constants are found in $LaAlO_3$ films of all thicknesses, one is close to that of the $SrTiO_3$ substrate and the other decreases continuously when the film thickness is above about 20 unit cells towards the value of bulk $LaAlO_3$. A rough estimate using the areas under each peaks reveals that the former layer is about 10 unit cells thick for all the $LaAlO_3$ films. A na¨ıve model to explain the result suggests that a thin LaAlO3 layer of 10 unit cells next to the $SrTiO_3$ substrate is nearly coherently strained, while the top part of the $LaAlO_3$ film relaxes as the film thickness increases above 20 unit cells.

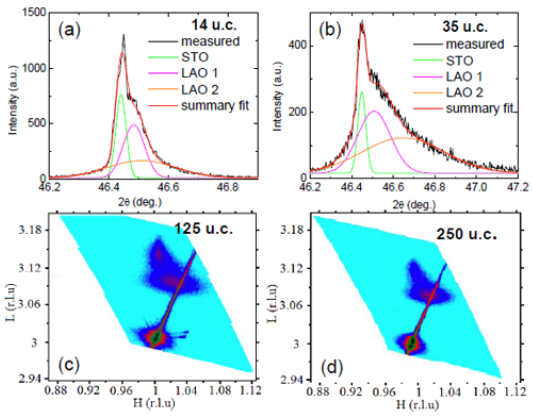

Figure 6: XRD measurements for 4 LaAlO3 films on SrTiO3. The thicknesses are (a) 14, (b) 35, (c) 125, and (d) 250 unit cells. (a) and (b) are the (200) plane diffraction measured by GIXRD. (c) and (d) are reciprocal space mapping around the SrTiO3 (103) reflection.

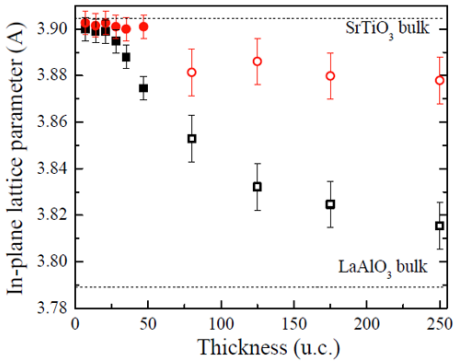

Figure 7: In-plane lattice constant of LaAlO3 films on SrTiO3 as a function of film thickness. The solid symbols are from GIXRD, and the open symbols are from RSM. The dotted lines are the bulk values for LaAlO3 and SrTiO3, respectively.

The strain relaxation in the $LaAlO_3$ films is accompanied by cracks. Figure 8 shows AFM images for the thicknesses of 7, 21, 35, and 125 unit cells. All the films show regularly-spaced steps of about 0.39 nm height, confirming that the films grew by the layer-by-layer mode. At the thickness of 21 unit cells, when the top layer starts to relax, the surface of the film begins to exhibit cracks. When the film thickness is beyond 125 unit cells the crack disappears and the films surface is smooth with clear terraces. Such behavior has been explained by Prof. Long-Qing Chen of Penn State University using the Griffith fracture theory [60]. The film cracks when the energy release rate G in the event of cracking is larger than the resistance of the material to cracking Gc. Based on the result in Fig. 7, G peaks between around 20 and 125 unit cells, within which G > Gc is satisfied, leading to cracks.

Electrical contacts to the 2DEG were made by depositing Cr/Au pads in contact holes to the $LaAlO_3/SrTiO_3$ interface, and the transport properties were measured. Below the $LaAlO_3$ thickness of 4 unit cells, the interface is insulating. Above 4 unit cells, the interface becomes conducting, and the conductivity changes with $LaAlO_3$ film thickness. In Fig. 9, the temperature dependencies of the sheet resistance Rs and carrier density ns of the $LaAlO_3/SrTiO_3$ interface are shown for different $LaAlO_3$ film thicknesses. A large drop in the sheet resistance and a large increase in the carrier density, both by 2 orders of magnitude, are seen when the film thickness is increased to 21 unit cells, the thickness when the top layer starts to relax. Clearly, the interface properties are closely related to the strain state in the $LaAlO_3$ films.

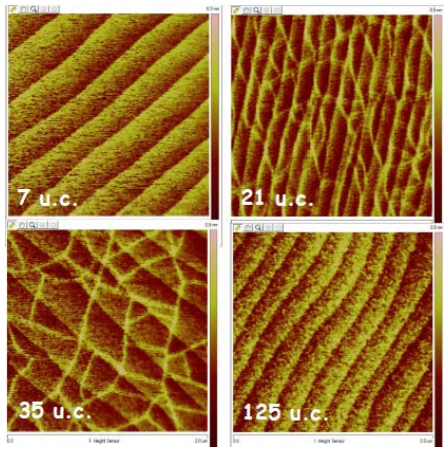

Figure 8: AFM images of $LaAlO_3$ films of different thicknesses. Cracks are seen in films above about 20 unit cells, which vanish when the film is thicker than about 125 unit cells.

The sheet resistance and carrier density of the interfacial 2DEG at 300 K as functions of $LaAlO_3$ film thickness dLAO are plotted in Fig. 10. For dLAO < 4 unit cells, the interface is insulating. Above 4 unit cells both Rs and ns are dependent on the $LaAlO_3$ film thickness. The sheet resistance decreases with increasing dLAO gradually until about 20 unit cells, when it drops sharply and remains relatively constant at larger dLAO. The carrier density increases with increasing dLAO towards the predicted value of 3.3 x 10^{14} cm^{-2} (half an electron per unit cell) before it jumps sharply at about 20 unit cells by 2 orders of magnitude. It remains constant at larger $LaAlO_3$ film thicknesses.

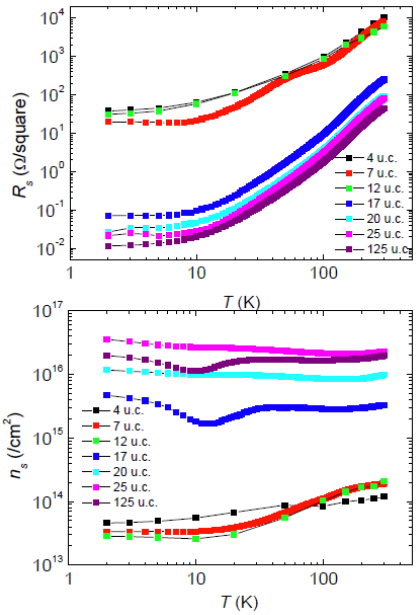

Figure 9: Temperature dependence of (a) sheet resistance and (b) carrier density of the2DEG at the $LaAlO_3/SrTiO_3$ interface for different $LaAlO_3$ film thicknesses.

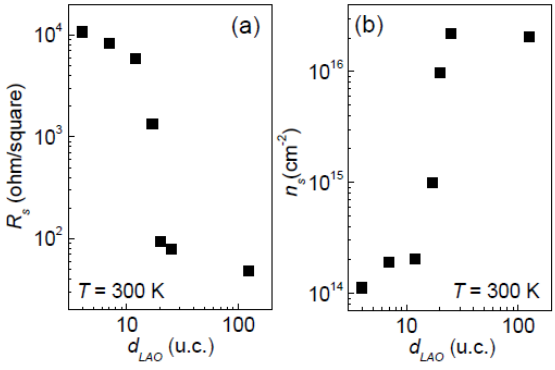

Figure 10: Dependence of (a) sheet resistance and (b) carrier density of the interfacial 2DEG at 300 K on the $LaAlO_3$ film thickness dLAO.

While the dLAO dependence of the sheet resistance and carrier density may confirm the incomplete charge screening that causes the potential buildup observed by Singh-Bhalla et al. [24] or indicate extrinsic origins of the conducting interface such as oxygen vacancies [20] or interfacial mixing [22], it is surprising to find that the thickness when the sudden changes in Rs and ns take place is the same as when the strain in the $LaAlO_3$ film starts to relax quickly and cracks appear in the film. Our result adds an important piece of information to the heated debate concerning the mechanism of the conducting interface between $LaAlO_3$ and $SrTiO_3$.

3 Publications in the current project period

Publications are being prepared on "Atomic layer-by-layer growth of homoepitaxial $SrTiO_3$ films by laser MBE from SrO and TiO_2 targets" and "Strain relaxation in $LaAlO_3$ films and its effect on the 2D electron gas at $LaAlO_3/SrTiO_3$ interface". Publications resulting from research performed at Penn State University: 1. A. Soukiassian, W. Tian, V. Vaithyanathan, J. H. Haeni, L. Q. Chen, X. X. Xi, D. G. Schlom, D. A. Tenne, H. P. Sun, X. Q. Pan, K. J. Choi, C. B. Eom, Y. L. Li, Q. X. Jia, C. Constantin, R.M. Feenstra, M. Bernhagen, P. Reiche, and R. Uecker, Growth of nanoscale $BaTiO_3/SrTiO_3$ superlattices by molecular-beam epitaxy, J. Mater. Res. 23, 1417 (2008). 2. Dmitri A. Tenne and Xiaoxing Xi, 8 Raman Spectroscopy of Ferroelectric Thin Films and Superlattices, J. Am. Ceram. Soc., 91, 1820 (2008). 3. Shufang Wang, A. Venimadhav, Shengming Guo, Ke Chen, Qi Li, A. Soukiassian, Darrell G. Schlom, Michael B. Katz, X. Q. Pan, Winnie Wong-Ng, Mark D. Vaudin, and X. X. Xi, Structural and thermoelectric properties of Bi2Sr2Co2Oy thin films on LaAlO3 (100) and fused silica substrates, Appl. Phys. Lett. 94, 022110 (2009). 4. D. A. Tenne, H. N. Lee, R. S. Katiyar, and X. X. Xi, Ferroelectric phase transitions in three-component short-period superlattices studied by ultraviolet Raman spectroscopy, J. Appl. Phys. 105, 054106 (2009). 5. D. A. Tenne, P. Turner, J. D. Schmidt, M. Biegalski, Y. L. Li, L. Q. Chen, A. Soukiassian, S. Trolier-McKinstry, D. G. Schlom, X. X. Xi, D. D. Fong, P. H. Fuoss, J. A. Eastman, G. B. Stephenson, C. Thompson, and S. K. Streiffer, Ferroelectricity in Ultrathin BaTiO3 Films: Probing the Size Effect by Ultraviolet Raman Spectroscopy, Phys. Rev. Lett. 103, 177601 (2009). 6. N. D. Lanzillotti-Kimura, A. Fainstein, B. Perrin, B. Jusserand, A. Soukiassian, X. X. Xi, and D. G. Schlom, Enhancement and Inhibition of Coherent Phonon Emission of a Ni Film in a $BaTiO_3/SrTiO_3$ Cavity, Phys. Rev. Lett. 104, 187402 (2010). 7. J. Hlinka, V. Zelezn´y, S. M. Nakhmanson, A. Soukiassian, X. X. Xi, and D. G. Schlom, Soft-mode spectroscopy of epitaxial BaTiO3/SrTiO3 superlattices, Phys. Rev. B 82, 224102 (2010). 8. A. F. Garca-Flores, D. A. Tenne, Y. J. Choi, W. J. Ren, X. X. Xi, and S. W. Cheong, Temperature-dependent Raman scattering of multiferroic Pb(Fe1=2Nb1=2)O3, J. Phys.: Condens. Matter 23, 015401 (2011). 9. A. Bruchhausen, A. Fainstein, S. Tinte, A. Soukiassian, D. G. Schlom, X. X. Xi, Coupling between Light and Terahertz-Frequency Acoustic Phonons in Ferroelectric $BaTiO_3/SrTiO_3$ Superlattices, Chin. J. Phys. 49, 159 (2011).

References

[1] D.G. Schlom, J. H. Hanei, J. Lettieri, C. D. Theis, W. Tian, J. C. Jiang, and X. Q. Pan, "Oxide nano-engineering using MBE", Mater. Sci. Eng. B 87, 282 (2001).

[2] H. Koinuma, N. Kanda, J. Nishino, A. Ohtomo, H. Kubota, M. Kawasaki, and M. Yoshimoto, “Laser MBE of ceramic thin films for future electronics”, Appl. Surf. Sci. 111, 514 (1997).

[3] H. Koinuma, “Chemistry and electronics of oxides from carbon dioxide to perovskite”, Thin Solid Films 486, 2 (2005).

[4] C. M. Brooks, L. Fitting Kourkoutis, T. Heeg, J. Schubert, D. A. Muller, and D. G. Schlom, “Growth of homoepitaxial SrTiO3 thin films by molecular-beam epitaxy”, Appl. Phys. Lett. 94, 162905 (2009).

[5] A. Soukiassian, W. Tian, V. Vaithyanathan, J. H. Haeni, L. Q. Chen, X. X. Xi, D. G. Schlom, D. A. Tenne, H. P. Sun, X. Q. Pan, K. J. Choi, C. B. Eom, Y. L. Li, Q. X. Jia, C. Constantin, R. M. Feenstra, M. Bernhagen, P. Reiche, and R. Uecker, “Growth of nanoscale BaTiO3/SrTiO3 superlattices by molecular-beam epitaxy”, J. Mater. Res. 23, 1417 (2008).

[6] D. A. Tenne, A. Bruchhausen, N. D. Lanzillotti-Kimura, A. Fainstein, R. S. Katiyar, A. Cantarero, A. Soukiassian, V. Vaithyanathan, J. H. Haeni, W. Tian, D. G. Schlom, K. J. Choi, D. M. Kim, C. B. Eom, H. P. Sun, X. Q. Pan, Y. L. Li, L. Q. Chen, Q. X. Jia, S. M. Nakhmanson, K. M. Rabe, and X. X. Xi, “Probing nanoscale ferroelectricity by ultraviolet Raman spectroscopy”, Science 313, 1614 (2006).

[7] A. Ohtomo and H. Y. Hwang, “A high-mobility electron gas at the LaAlO3/SrTiO3 heterointerface”, Nature 427, 423 (2004).

[8] Tsuyoshi Ohnishi, Keisuke Shibuya, Takahisa Yamamoto, and Mikk Lippmaa, “Defects and transport in complex oxide thin films”, J. Appl. Phys. 103, 103703 (2008).

[9] M. Kanai, T. Kawai, and S. Kawai, “Atomic layer and unit-cell growth of (Ca,Sr)CuO2 thin films by laser molecular-beam epitaxy”, Appl. Phys. Lett. 58, 771 (1991).

[10] M. Kawasaki, K. Takahashi, T. Maeda, R. Tsuchiya, M. Shinohara, O. Ishiyama, T. Yonezawa, M. Yoshimoto, and H. Koinuma, “Atomic control of the SrTiO3 crystal surface”, Science 266, 1540 (1994).

[11] Gertjan Koster, Boike L. Kropman, Guus J. H. M. Rijnders, Dave H. A. Blank, and Horst Rogalla, “Quasi-ideal strontium titanate crystal surfaces through formation of strontium hydroxide”, Appl. Phys. Lett. 73, 2920 (1998).

[12] M. Basletic, J.-L. Maurice, C. Carr´et´ero, G. Herranz, O. Copie, M. Bibes, ´E. Jacquet, K. Bouzehouane, S. Fusil, and A. Barth´el´emy, “Mapping the spatial distribution of charge carriers in LaAlO3/SrTiO3 heterostructures”, Nature Mater. 7, 621 (2008).

[13] N. Reyren, S. Thiel, A. D. Caviglia, L. Fitting Kourkoutis, G. Hammerl, C. Richter, C. W. Schneider, T. Kopp, A.-S. Retschi, D. Jaccard, M. Gabay, D. A. Muller, J.-M. Triscone, and J. Mannhart, “Superconducting interfaces between insulating oxides”, Science 317, 1196 (2007).

[14] A. Brinkman, M. Huijben, M. Van Zalk, J. Huijben, U. Zeitler, J. C. Maan, W. G. Van Der Wiel, G. Rijnders, D. H. A. Blank, and H. Hilgenkamp, “Magnetic effects at the interface between non-magnetic oxides”, Nature Mater. 6, 493 (2007).

[15] Pavlo Zubko, Stefano Gariglio, Marc Gabay, Philippe Ghosez, and Jean-Marc Triscone, “Interface physics in complex oxide heterostructures”, Annu. Rev. Condens. Matter Phys. 2, 141 (2011).

[16] Darrell G. Schlom and Jochen Mannhart, “Interface takes charge over Si”, Nature Mater. 10, 168 (2011).

[17] Naoyuki Nakagawa, Harold Y. Hwang, and David A. Muller, “Why some interfaces cannot be sharp”, Nature Mater. 5, 204 (2006).

[18] J. Mannhart and D. G. Schlom, “Oxide interfaces – an opportunity for electronics”, Science 327, 1607 (2010).

[19] S. Thiel, G. Hammerl, A. Schmehl, C. W. Schneider, and J. Mannhart, “Tunable quasi-two-dimensional electron gases in oxide heterostructures”, Science 313, 1942 (2006).

[20] Wolter Siemons, Gertjan Koster, Hideki Yamamoto, Walter A. Harrison, Gerald Lucovsky, Theodore H. Geballe, Dave H. A. Blank, and Malcolm R. Beasley, “Origin of charge density at LaAlO3 on SrTiO3 heterointerfaces: Possibility of intrinsic doping”, Phys. Rev. Lett. 98, 196802 (2007).

[21] Keisuke Shibuya, Tsuyoshi Ohnishi, Mikk Lippmaa, and Masaharu Oshima, “Metallic conductivity at the CaHfO3/SrTiO3 interface”, Appl. Phys. Lett. 91, 232106 (2007).

[22] P. R. Willmott, S. A. Pauli, R. Herger, C. M. Schlep¨utz, D. Martoccia, B. D. Patterson, B. Delley, R. Clarke, D. Kumah, C. Cionca, and Y. Yacoby, “Structural basis for the conducting interface between LaAlO3 and SrTiO3”, Phys. Rev. Lett. 99, 155502 (2007).

[23] C. Bell, S. Harashima, Y. Hikita, and H. Y. Hwang, “Thickness dependence of the mobility at the LaAlO3/SrTiO3 interface”, Appl. Phys. Lett. 94, 222111 (2009).

[24] Guneeta Singh-Bhalla, Christopher Bell, Jayakanth Ravichandran, Wolter Siemons, Yasuyuki Hikita, Sayeef Salahuddin, Arthur F. Hebard, Harold Y. Hwang, and Ramamoorthy Ramesh, “Built-in and induced polarization across LaAlO3/SrTiO3 heterojunctions”, Nature Phys. 7, 80 (2011).